Mixed dimensionality quantum heterostructures grown in axially modulated V grooves

B. Dwir, K. Leifer, and E. Kapon
Laboratory for Physics of Nanostructures, Institute of Quantum Photonics and Electronics (IPEQ), Faculty of Basic Sciences, Swiss Federal Institute of Technology Lausanne (EPFL), CH-1015 Lausanne, Switzerland
(Received 24 May 2002; revised manuscript received 27 September 2002; published 5 February 2003)

We developed low-dimensional AlGaAs/GaAs heterostructures, which combine quantum well (QW), quantum wire (QWR), and quantum dot (QD) like structures along the bottom of a single V groove. By varying the groove geometry (through the use of electron-beam lithography), we could modify the morphology and control the size of each part of the grown structure on a submicron scale. We characterized the growth by cross-sectional atomic force microscopy and established the relation between substrate shape and growth front as function of grown thickness, as well as the formation of QWs and QWRs. In particular, we demonstrated the possibility to obtain a thicker, short QWR section in the center of a widening in a V-groove QWR. We confirmed the structural features, and specifically the lower band gap of the QD-like section, by low-temperature microphotoluminescence and cathodoluminescence spectroscopies.

DOI: 10.1103/PhysRevB.67.075302 PACS number(s): 68.65.Hb, 68.65.La, 73.21.La, 73.21.Hb

I. INTRODUCTION

Quantum wire (QWR) semiconductor structures, which utilize two-dimensional (2D) quantum confinement of electrons and holes, have attracted considerable interest because of the physics they exhibit, as well as their unique features useful for electronic and optoelectronic device applications.[1,2] Most of the experimental effort in this domain has been devoted, however, to nominally uniform QWR structures, in which the confining potential profile is ideally kept constant along the wire's axis. Several useful approaches for realizing uniform QWR structures suitable for 1D system investigations and device applications have been identified so far. The most successful approaches have relied on the *in situ* formation of the wire interfaces to ensure their high quality. The first *in situ* growth methods used vicinal GaAs surfaces, especially the (311)*A* surface, to form dense (3–20-nm pitch) arrays of QWRs on nanofaceted surfaces that spontaneously form during growth.[3–5] However, fluctuations in the nanofaceted structure[4] lead to relatively large disorder in the resulting QWRs, resulting in wide photoluminescence peaks.[5] Moreover, the high density of QWRs in these arrays does not allow to isolate a single QWR, e.g., for transport applications. Other successful approaches to the fabrication of high-quality, homogeneous single (or arrays of) QWRs included using cleaved edge overgrowth[6] and self-ordering on V-grooved substrates.[7,8] Both types of QWRs have shown 1D density of states in optical spectroscopy as well as quantized conductance step transport experiments.

During the last years, good theoretical understanding of the self-limited growth mechanisms in V grooves has been achieved.[9,10] Although the self-limited profile is independent of the initial form of the V groove, it has been shown that *along the wire* there always exist monolayer steps, spaced by a few hundred nanometers, as well as larger (few nanometers) jumps, spaced by 1–2 μm.[10] These steps and jumps induce random fluctuations in the confinement potential *along* the wire, which result in random fluctuations in the QWR subbands *along* the wire. The magnitude of these fluctuations is important enough to limit the electron mean free path in transport experiments[11] and cause exciton localization, observable in optical spectroscopy experiments.[8,12] However, the random nature of the steps and jumps does not provide a way of controlling their placement, extent, or strength, thus limiting their usefulness in research or for applications.

On the other hand, QWRs in which this potential varies in a *controlled* fashion along the axis of the wire would offer approaches for modifying the electronic band structure, leading to optical and transport properties. Several examples of such axially modulated waveguides and wires have been considered theoretically, including curved and twisted wires,[13,14] sharp bends,[15] single and double 90° wire bends,[16–19] width changes and stubs,[19] and multiple ports.[20] Periodically modulated QWRs have been shown to produce gaps in plasmon dispersion[21] and lead to localization effects.[22] In all these structures, either the 1D nature of the carriers is maintained, or 1D-0D transitions are induced (as in bent wires), leading to localization or to the formation of effective quantum dots (QDs). In this context of changing dimensionality, 2D-1D transitions should also be considered. As one motivation, we recall that the analysis of transport properties of electrons in uniform QWRs has recently shown the importance of the quantum well QW/QWR (2D/1D) interface as a source of contact resistance,[7,23] which could be reduced or eliminated by using adiabatic transition between QW and QWR. The possibility of realizing such adiabatic contacts by varying the QWR structure along its axis is therefore very important for future study of transport in QWRs with strong confinement potential. In the domain of pure 1D confinement, we mention as an example that the study of exciton transport along QWRs could also benefit from the possibility of varying the confinement potential (i.e., the band gap) along the wire, which could lead to controlled acceleration of carriers (electrons or excitons).

Attempts to realize axially modulated 1D wires have so far been rather limited, mainly due to the technological difficulties involved. Several tests of theoretical predictions have been performed in electron waveguides,[15,17,18] by mea-

suring conductivity in gated[18–20,24] or etched[25,26] QW structures. However, in gated structures the confinement potential is rather weak, and there is no independent control of the confinement potential and wire shape. Etched structures, on the other hand, exhibit large scattering due to the etched interfaces, and are limited in size and potential abruptness by surface states.

In this paper, we present an approach for the realization of various types of modulated QWR structures, which combines the advantages of V-groove growth (self-ordering, the formation of a well-controlled QWR of nanometer-sized dimensions at the bottom of the groove) with those of nanolithography (control over position on a sub-μm scale), to produce high-quality, well-controlled structures of mixed dimensionality. In this approach, we use the dependence of the evolution of growth in a groove on the groove's shape to generate controlled variations in a QWR along its axis by modulating the shape of the V groove. A 3D structure reconstruction, using cross-sectional atomic force microscopy (AFM),[27] yields the details of the 3D growth with nanometer spatial resolution and permits the identification of several types of nanostructures: QWs, QWRs, and QD-like short QWR segments. The evolution of both structural features and the band gap are further studied by growing a single GaAs/AlGaAs heterostructure, which is then characterized by AFM, photoluminescence, and cathodoluminescence (CL) spectroscopies.

II. SUBSTRATE FEATURES

Our electron-beam lithography (EBL) technique and the details of substrate preparation and organometallic chemical vapor deposition (OMCVD) growth have been presented elsewhere.[28] To produce variable-width V grooves, we first write by EBL, on a (100) GaAs substrate, an array of open variable-width lines in a PMMA resist layer,[28] oriented in the $[01\bar{1}]$ direction. Wet chemical etching (using the anisotropic etchant $H_2SO_4:H_2O_2:H_2O$) of the substrate through the open lines leads to the formation of an array of V grooves, whose widths vary along their axes, as can be seen in the top AFM image of a substrate [Fig. 1(a)]. Analysis of the substrate profile across [Figs. 1(b) and 1(c)] and along [Fig. 1(d)] the grooves reveals that the groove has indeed a V shape at the narrow part, with a top width of 0.3 μm. The wide part has a top width of 0.65 μm and flat bottom width of 0.2 μm. The depths of the two parts are not equal, the narrow and wide parts being 0.25- and 0.4-μm deep, respectively. This is a consequence of the anisotropic etching process. The length of the wide part is 0.7 μm at the top and 0.4 μm at the bottom. Due to the high resolution of the EBL process, and the faceting of GaAs, the substrate exhibits a relatively abrupt transition from a narrow to wide groove, over a length of 0.2 μm, which will promote the formation of intermediate (e.g., {311}) crystalline planes between the {111} facets of the V-groove sidewalls and the {100} planes of the flat bottom.

III. STRUCTURE AND MORPHOLOGY

To investigate the growth features of AlGaAs and GaAs in variable-width V grooves, we grew a thick superlattice, made of alternating 5-nm GaAs and 24-nm $Al_{0.3}Ga_{0.7}As$ (nominal) layers, on the patterned substrate, using low pressure OMCVD.[9] The array of patterned grooves (2-μm pitch) was positioned in the (100) plane with a 1.2° angle to the $[01\bar{1}]$ direction [Fig. 1(e)], so as to produce a staggered array in which the wide part in the groove is shifted (along the wire) by 21 nm from one line to the next. In this way, cleaving the sample after growth allows to scan a sequence of AFM cross-sectional images of the grooves, where moving from one groove to the next is equivalent to probing the structure *along* the modulated groove, at 21-nm intervals. The different oxidation rates in air of AlGaAs with different Al contents give rise to the contrast necessary for observing the growth evolution.[27] The complete series of 100 grooves thus allows to probe the entire length of the structure, which repeats every 2 μm.

A sample of six AFM cross-sectional images are shown in Figs. 2(A)–2(F); these were taken at several positions along the groove, spanning the region between the center of the wide part and the narrow part, as indicated by the lines A–F in Fig. 1(a). The GaAs layers, of dark contrast, sandwiched between AlGaAs layers, of light contrast, are numbered 1–10 in Fig. 2. The measured thickness of a GaAs/AlGaAs layer pair is ~50 nm at the bottom of the narrow groove and ~35 nm in the planar regions, about 20% higher than the nominal thickness. The relatively thin GaAs layers show the evolution of the growth front, enabling us to visualize the different crystalline planes which form at different stages of the growth.

Study of the evolution of the growth planes in the wide, intermediate, and narrow parts of the groove at different heights from the substrate leads to the following observations:

(i) In the narrow groove [Fig. 2(F)] the self-limiting AlGaAs growth[9] leads to the formation of a sharp V-shaped growth front, with planes close to {111}*A*. GaAs growth leads to the formation of a crescent-shaped QWR, exactly in the same manner as in a uniform V groove. This structure maintains itself up to at least 500-nm total thickness. Measurements of the GaAs layer thickness at the center of the groove show an almost constant thickness of 14 nm for all layers (for 5-nm nominal thickness), a value similar to QWR thickness in uniform V grooves.

(ii) In the widest part of the groove [Fig. 2(A)], the flat bottom leads to planar (100) AlGaAs growth, on which a thin GaAs (100) QW (thickness≈7 nm) forms, with some GaAs thickening at the corner, where the transition to the side {111}*A* QWs occurs (layers 1–6). The higher-index planes ({311}*A* and {111}*A*) eventually catch up and reduce the width of the {100} region. At about 350 nm from the bottom of the groove, this reduction is followed by considerable thickening in the GaAs QW (up to 20 nm), which is now surrounded by {111}*A* planes, due to coalescence of the thicker QW edges (layers 7 and 8). Finally, at a total thickness of 450 nm, we observe a thick crescent-shaped QWR

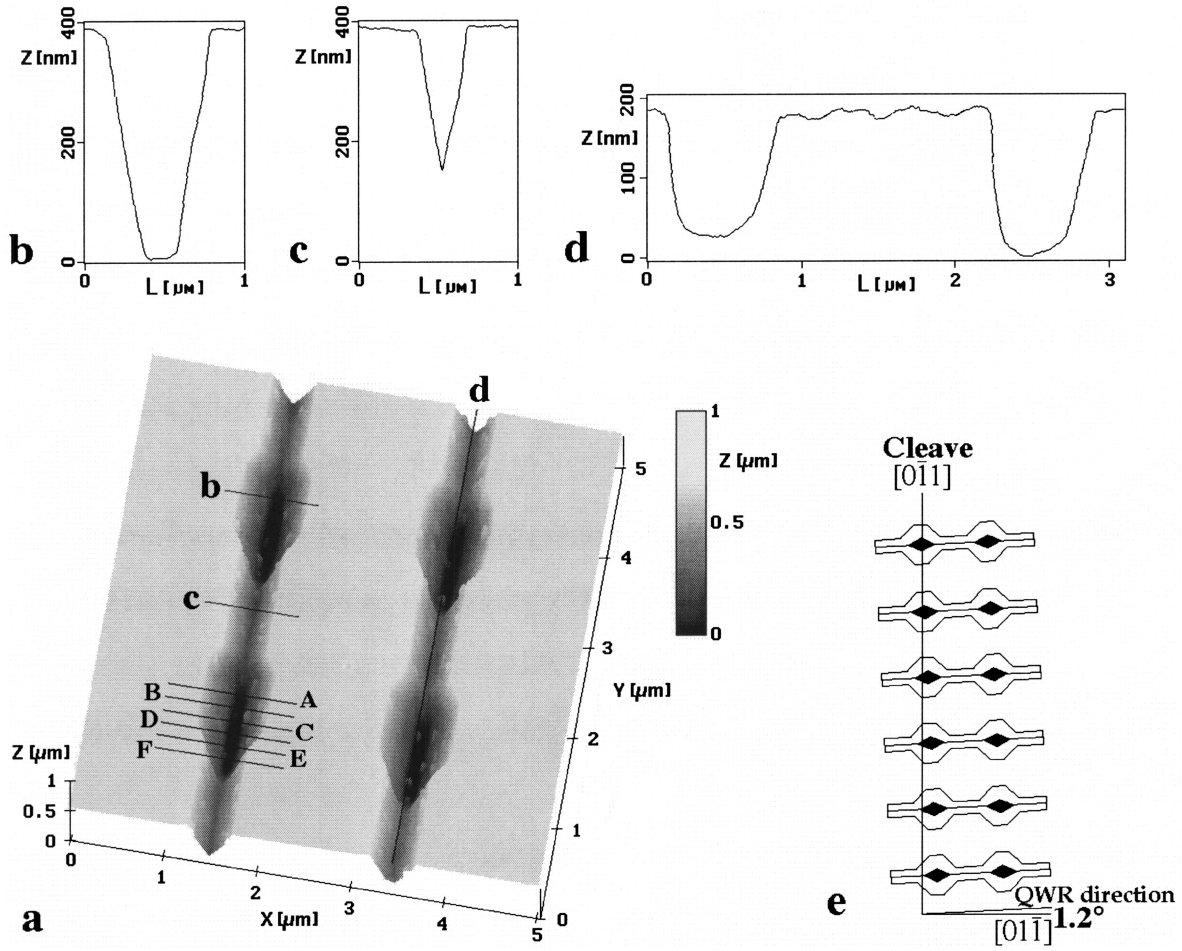

FIG. 1. (a) AFM image of a substrate with a 2-μm-pitch variable-width V-groove array. The lines b–d denote cross sections across and along the grooves, with corresponding profiles shown separately in graphs (b)–(d), respectively. The schematic (e) shows the principle of cross-sectional AFM sequencing, based on a series of tilted grooves (at 1.2° to the crystal direction $[01\bar{1}]$), which then produce a sequence of shifted AFM images in a single cleave. Lines A–F in (a) denote the positions along the groove of the AFM images, which are depicted in Fig. 2 below.

(layers 9 and 10). The QWR thickness (37 nm) is almost three times the usual self-limited GaAs QWR thickness (14 nm), probably due to extra Ga diffusion *along* the structure, which does not occur in uniform V grooves.[9,28]

(iii) Cross sections at intermediate distances from the center of the wide part of the groove show a gradual transition between the extreme cases of Figs. 2(A) and 2(F). An interesting intermediate state occurs when the {311}*A* facets replace the {111}*A* ones at the bottom of the groove [upper layers in Figs. 2(D) and 2(E)]. In this case, the GaAs layer does not show any thickening at the center of the groove. However, effective 2D quantum confinement can still be maintained in such a V-shaped QW layer through the Ga-rich AlGaAs barrier at the central part of the groove,[9] as well as by electrostatic effects of the curved shape of the layer.[29]

Another way to visualize this 3D structure is to reconstruct the development *along the groove* of the shape of a GaAs layer deposited on a buffer layer of a certain thickness. Layers deposited on a thin buffer (e.g., layers 1–3 in Fig. 2, up to about 150 nm from the bottom) show at the center of the wide groove a QW structure, with two thicker QWR-like parts at the edges, where the {100} and {111}*A* planes meet. Moving along the structure towards the narrow part, the QW becomes narrower, until the two side QWRs fuse together to form a single QWR at the center of the narrow V groove. This situation is somewhat modified when the buffer is thicker (e.g., layers 4–6 in Fig. 2, at 200–300 nm from the bottom), since the initial wide part is already narrower. The QW therefore disappears at a smaller distance from the center of the wide part, leading to the formation of {311} planes meeting at the bottom of the groove as an intermediate structure between the coalescing QWRs close to the center and the regular QWR forming at the narrow part. At a still higher position (buffer thickness$\sim$450 nm, e.g., layers 7–10 in Fig. 2), no QW is formed at the center of the wide part; instead, a very thick QWR section is formed there, which transforms to {311} QWs, then finally to a regular QWR in the narrow part. All these structural changes occur on a relatively short length scale (a few hundred nanometers), and lead to significant changes in the thickness of a deposited GaAs layer. These

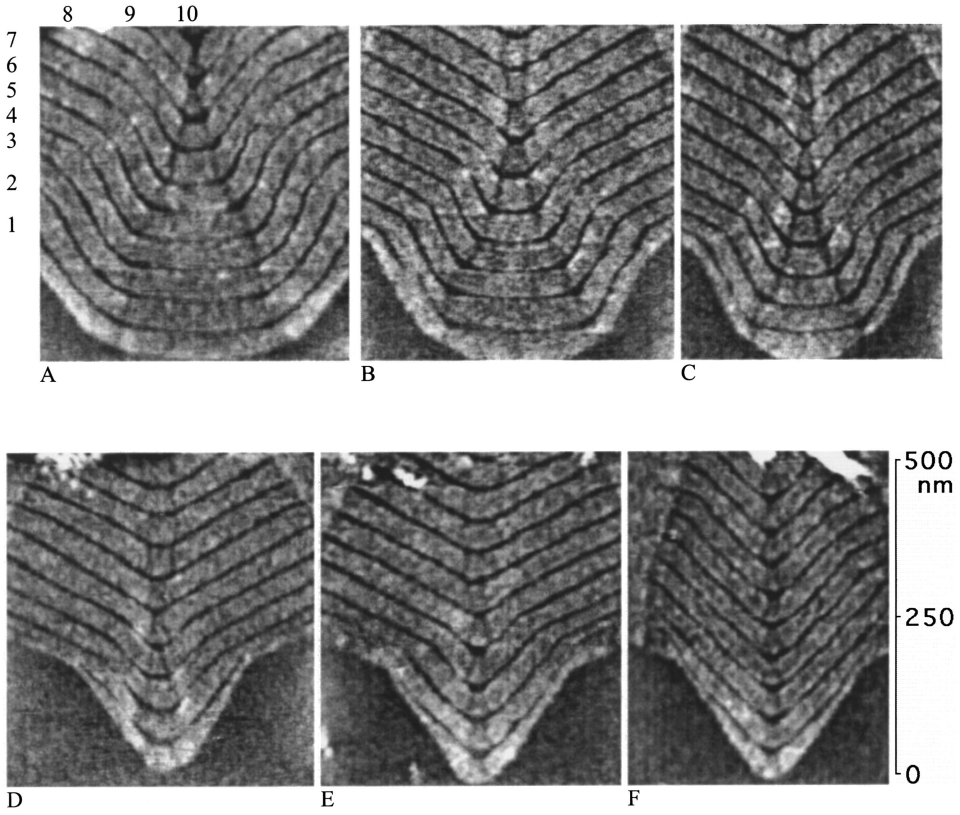

FIG. 2. A sequence of AFM cross-sectional images of an AlGaAs/GaAs multilayer structure grown on a 2-μm-pitch variable-width QWR array. Distance from the center of the wide region is (A) 0, (B) 130, (C) 240, (D) 300, (E) 435, and (F) 500 nm. The image height is 500 nm for all the images [scale on right of (F)], and the GaAs layers (dark contrast) are numbered from 1 to 10 [top left of (A)].

thickness variations would lead to significant energy-gap changes in thin AlGaAs/GaAs heterostructures grown in these grooves.

To analyze more quantitatively the changes in GaAs thickness along the wire, we plot in Fig. 3 the thickness of the 10 GaAs layers at the *bottom (center) of the groove* as a function of the distance along the groove. The data were measured from a sequence of 13 AFM cross sections, which represent a total distance of ± 500 nm from the center of the QWRs wide part. At the left and right extremes (where the V groove is narrow and regular QWRs are formed) we observe the usual self-limited QWR thickness of 14 nm, independent of layer number. In the central (wide) part of the groove, however, we see that the first five layers have all the same and almost constant thicknesses (about 7 nm). Layers 7 and 8 show each two 100-nm-long sections of an increased thickness (25 nm) at specific positions along the QWR. These sections correspond to the thickened QWs as in Fig. 2(B), layers 7 and 8. The top layer shows a much-increased thickness (37 nm) at the central part of the groove, along a section of about 100 nm. This section corresponds to the thicker crescent-shaped QWR in Fig. 2(A), layer 10. This QWR is almost three-times thicker than the one formed in the narrow V groove.

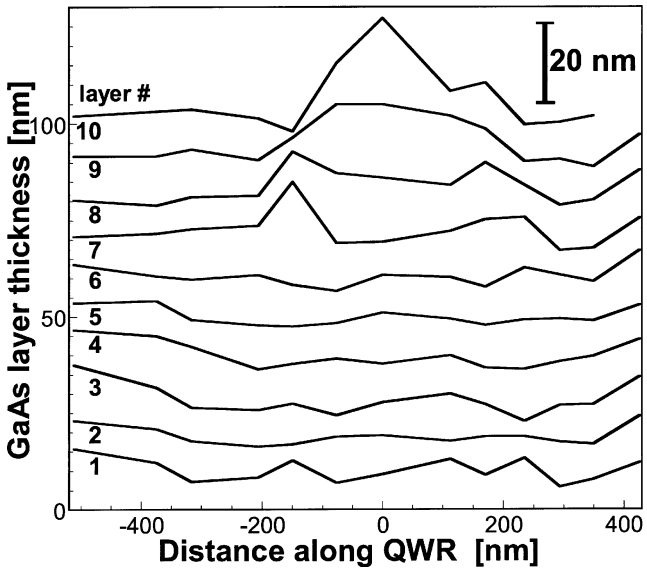

FIG. 3. Thickness of the GaAs layers (dark layers in Fig. 2), as measured from a sequence of 13 AFM cross-sectional images spanning almost 1 μm along the QWR. The graphs for the 10 GaAs layers have been shifted vertically by 10 nm for clarity, and the point $x=0$ denotes the center of the wide region.

The GaAs marker layers grown and characterized in the previous discussion are too thick to show distinctive photoluminescence peaks of the QWRs. To be able to easily distinguish the QWR peak, and especially to be able to separate the ''normal'' from the thick QWR peaks, a single GaAs layer should be used, and its thickness should be as small as possible; we chose to use a value of 1.5 nm (nominal thickness). Such thin GaAs layer is not visible in AFM cross sections, but we could still use the AFM to obtain a *top view* of the structure. Such imaging of the top surface is of course indicative of a single AlGaAs thickness (the total thickness of the growth), so we had to use separate growths in order to image different feature heights. We grew three samples

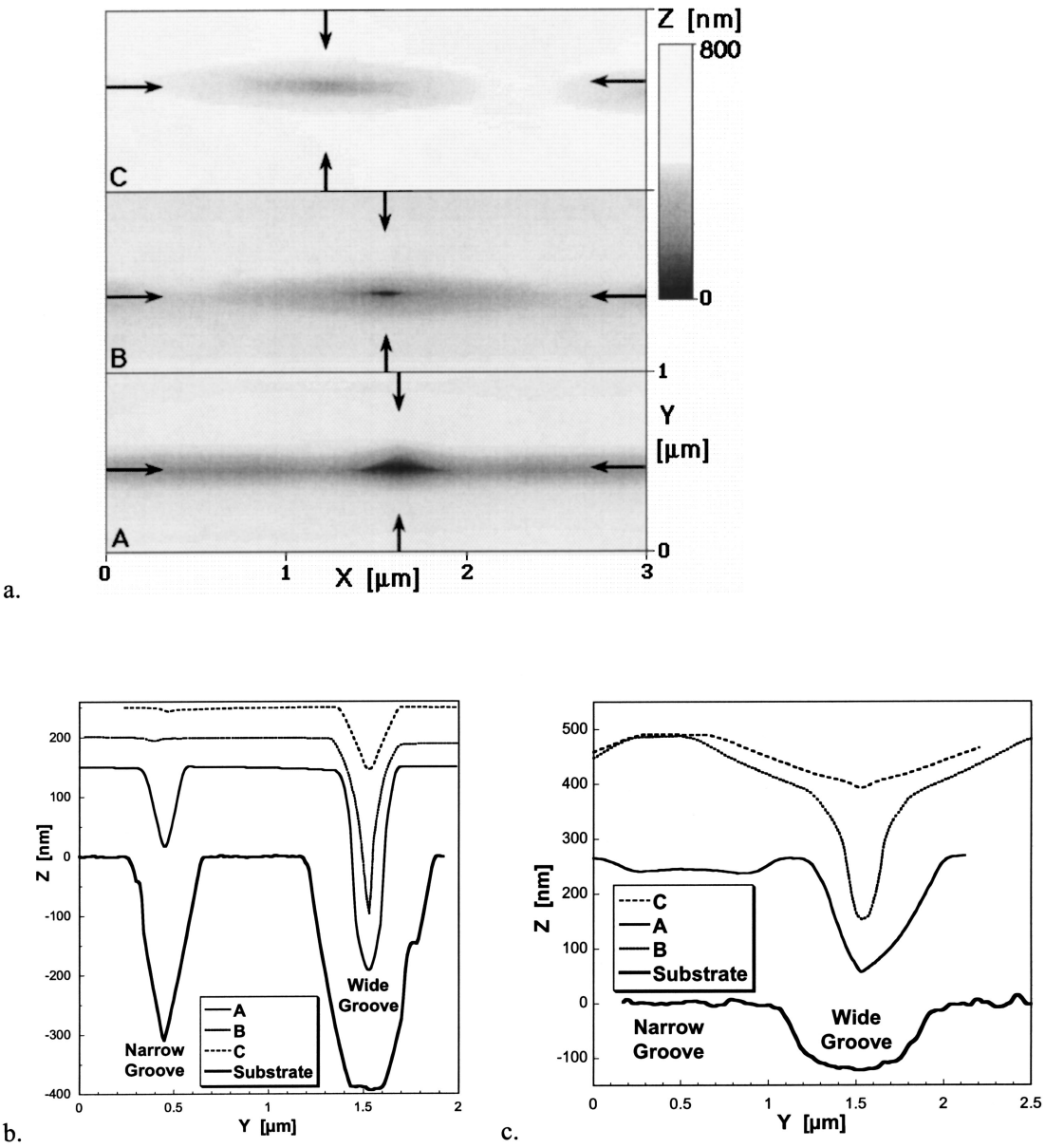

FIG. 4. (a) Top AFM images of (a) 200, (b) 250, and (c) 300 nm of AlGaAs (capped with 1.5-nm GaAs) grown in a variable-width V groove. The arrows denote the positions where line profiles of the top surfaces are shown across the grooves (b) and along the grooves (c), in the positions marked by arrows in (a). All line plots are relative to the substrate ($Z=0$, bottom line), and contain both a narrow and a wide part of the groove, as indicated.

(A–C), containing an AlGaAs buffer of nominal thicknesses 200, 250, and 300 nm, respectively, followed by a 1.5-nm GaAs cap. These nominal thicknesses correspond to the top of GaAs layer numbers 7, 9, and 11 in Figs. 2 and 3, respectively. In Fig. 4 we show top view AFM images of these samples, as well as the surface profiles derived from these images. A few structural features are evident: the planarization of the structure occurs first in the narrow part (between 200- and 250-nm buffer thickness), while the wide part does not planarize even at 300 nm. Still more interesting is the significant *shortening* of the widened region of the V groove, from ~500 nm in sample A, to ~150 nm in sample B, and ~100 nm in sample C, as can be seen in the profile plots [Figs. 4(b) and 4(c)]. This important shortening, coupled with the thickening of the GaAs layer, can lead to the formation of a QD-like structure, which will confine electrons and holes by the combined effect of composition and thickness variations, leading to a lower effective energy level with respect to both the surrounding AlGaAs (=lateral confinement) and neighboring QWR (=longitudinal confinement) and length (=quantized longitudinal states).

From Figs. 2–4 we see that, for an AlGaAs buffer thickness of >250 nm, a short and thick QWR section is formed at the center of the widened groove region. According to the

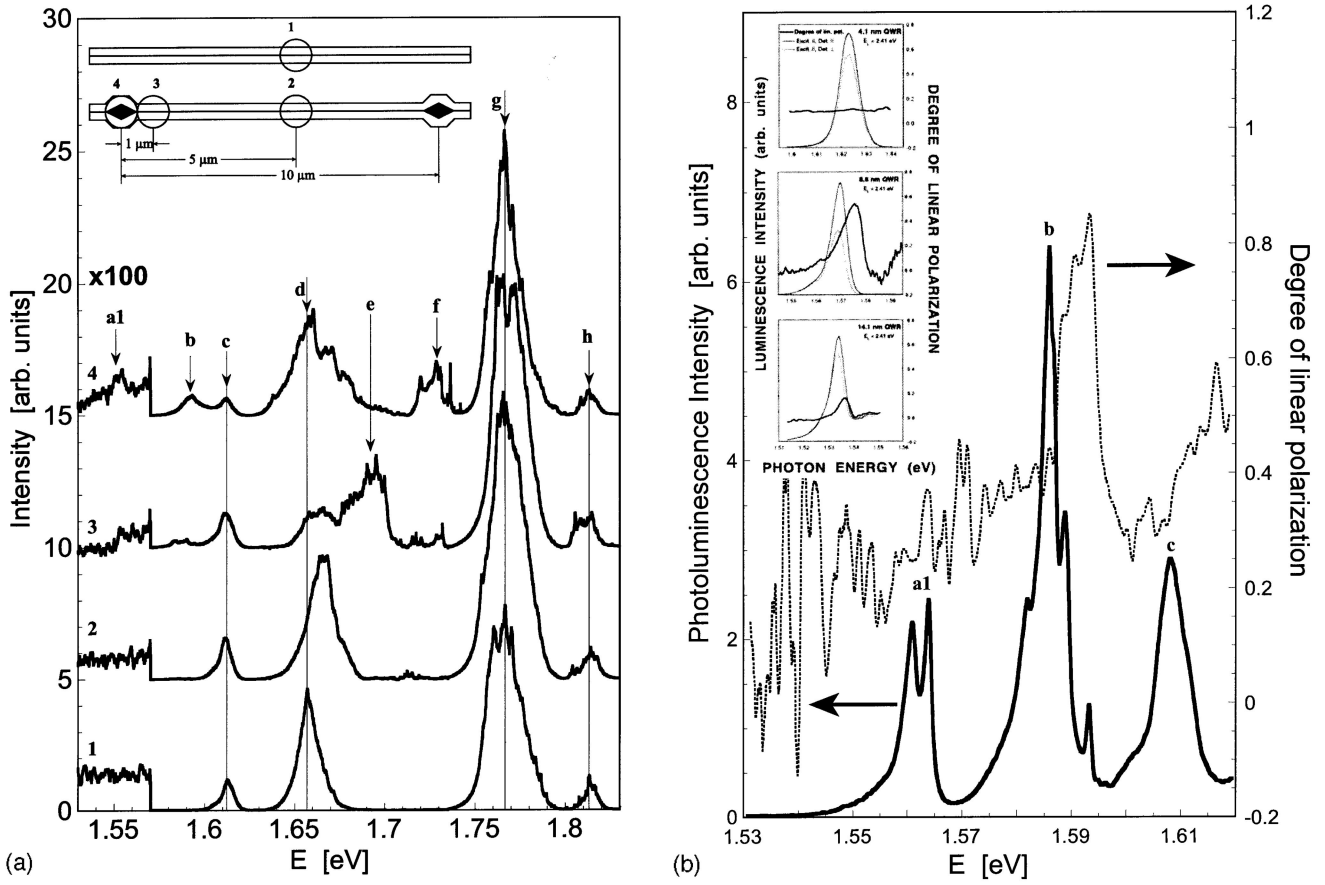

FIG. 5. (a) PL spectra at $T=10$ K, taken at four different positions along a uniform QWR (curve 1) and a variable-width structure (curves 2–4), as indicated in the inset diagram (the circles shows the approximate size of the PL excitation beam, 1 μm; the wide QWR size is exaggerated). The arrows marking a–g denote peaks and groups of peaks that are referred to in the text. (b) PL spectrum at $T=10$ K, taken at position (curve 4) in (a), with long integration time (full line). The dotted line represents the degree of linear polarization of the luminescence signal. Inset: PL spectra (thin line) and degree of polarization (thick line) for three uniform QWRs of thicknesses 4.1, 8.8, and 14.1 nm (from Ref. 31).

cross-sectional AFM images, its width and height are about 24 and 7.5 times the nominal grown GaAs thickness, respectively. Therefore, for a 1.5-nm nominal GaAs layer, as grown in samples A–C (Fig. 4 and the luminescence spectra) we expect the QWR dimensions to be $\sim 100\times 35\times 11$ nm (length$\times$width$\times$height), small enough to confine carriers as an effective QD (and too small to be observable by AFM). This structure corresponds to the thickened short QWR seen at layers 9 and 10 in the cross section, Fig. 2(A). We can thus use a narrow V groove with a short wide part as a template for making a QD connected on both sides to QWRs. Alternatively, from the observation of the lower layers of Fig. 2, we can also suggest another method for obtaining short GaAs QWR sections: They could be formed at the bottom of a narrow groove section, between two adjacent wider groove sections, when grown on a thin AlGaAs buffer (e.g., 100 nm). In this case, the short section would be of the usual QWR type [grown in a narrow V groove, Fig. 2(F)], and it would be coupled to planar (100) QWs, possibly with thickened edges [Figs. 2(A)–2(C)]. Such structures have been grown on V grooves tapered along several micrometers and have indeed shown the predicted structural features.[30]

IV. OPTICAL CHARACTERIZATION

For luminescence studies we grew a variable-width QWR structure with a single GaAs layer of nominal thickness 1.5 nm, sandwiched between an AlGaAs buffer layer of 250-nm (nominal) thickness and a top 50-nm (nominal) AlGaAs layer. The surface of the GaAs layer in this structure corresponds approximately to the surface of the sample depicted in Fig. 2, layer 9, and in Fig. 4, sample B. In this way, the luminescence studies are performed on samples whose morphology has already been characterized. Low-temperature (10 K) microphotoluminescence (μPL) measurements were performed on this structure, using an Ar^+-ion laser emitting at 514-nm wavelength with a spot size of <1 μm as excitation source, and a single 50-cm monochromator with charge coupled device camera as detector.

Figure 5(a) shows a series of μPL spectra taken at different positions on a variable-width QWR structure (curves 2–4), part of an array of 5-μm longitudinal pitch, as well as on a uniform narrow V groove (curve 1), part of an array of uniform structures grown simultaneously and on the same substrate. In the energy range of interest, 1.53–1.83 eV, we

distinguish many features, denoted by letters a–h on top of (a). The uniform QWR luminescence spectrum [Fig. 5(a) curve 1] comprises the peaks c, d, g, and h. These peaks have already been observed in many uniform V-groove samples of similar GaAs thickness and Al mole fraction.[31] Their identification is therefore straightforward: peak c corresponds to luminescence from the QWR, peak d to the side (thicker) {311} QWs, the group of peaks g to the side ({111}) and top QWs, and peak h to the vertical QW. The vertical QW peak h confirms the grown Al mole fraction in the sample (31.5%). The relatively narrow (7-meV) QWR peak c shows the good uniformity of the sample on the scale of the μPL measurement (a few micrometers). Note that peaks c, g, and h appear in all other spectra as well, sometimes with slight energy shifts (a few meV). Peak d also appears in all spectra, but its position varies between samples, consistent with the fact that the {311} planes are varying in thickness between narrow, wide, and intermediate parts of the groove.

Spectrum 2, taken in the middle of the narrow part of the structure (i.e., 2.5 μm away from the wide part), is almost identical to spectrum 1. Small variations in peak g, as well as a marked change in peak d, might show the influence of longitudinal diffusion of adatoms during growth on the thickness of the {311} planes and side ({111}) QWs.

Spectrum 4, taken at the center of the wide part, shows a few extra peaks (a1, b, and f), which are absent in spectra 1 and 2. The most intriguing is the weak low-energy peak a1 at 1.55 eV, which we assign to luminescence from the thicker QWR section at the center of the wide part of the V groove [Fig. 2(A), layers 9 and 10 and Fig. 4, sample B]. As we show below, this assignment fits well with the structural data, and is also supported by CL imaging. Peak b is the ''usual'' QWR peak (c), coming from narrow regions outside the wide groove, as we see below, but downshifted in energy, probably showing QWR thickening due to adatom diffusion during growth. The PL spot is large enough to show both peaks b and c at the central part of the wide regions; to better distinguish their source we use the CL technique described below. Finally, peak f is probably related to the narrow {311} QW at the intermediate region next to the wide part. Spectrum 3, taken at about 1 μm from the wide part, shows essentially the same features as the combined spectra 2 and 4, as expected.

A more detailed spectrum of the wide QWR region, measured with lower excitation intensity [0.1 vs 10 μW in Fig. 5(a)] and longer integration time, is shown in Fig. 5(b). Peaks a1, b, and c are again clearly seen, in the same position as in the previous spectrum, but are more easily resolved. Peak a1 is split in two; we suppose that this splitting of 3 meV could be due to exciton localization in the relatively long (80–100-nm) thick QWR section. Looking at the polarization data, we note that both peaks a1 and c do not show any polarization anisotropy, while peak b does. When comparing with data from Ref. 31 [inset, Fig. 5(b)], we note that thin QWRs (top curve in the inset and our peak c) do not show significant polarization, while thicker QWRs do (middle and bottom curves in inset, our peak b). This is explained by larger disorder in the thin QWRs, leading to stronger localization of the excitons.[12,31] In our sample, we could thus interpret the absence of polarization anisotropy in the thickest structure (peak c) as an indication of exciton localization, i.e., the formation of QD-like states.

V. CATHODOLUMINESCENCE CHARACTERIZATION

To identify the structural origin of the photoluminescence peaks with a higher spatial resolution, we performed cathodoluminescence (CL) spectroscopy on the same sample. The CL measurements were carried out on a Cambridge S-360 scanning electron microscope (SEM) equipped with a He-cooled stage (10 K) at an acceleration voltage of 5 kV and an electron-beam current of 1 nA. In Fig. 6(a) we show three CL spectra, taken at positions on the sample similar to the positions where PL spectra were taken: spectrum 1 is from a uniform V groove, spectrum 3 from the center of the wide region, and spectrum 2 from about 1 μm away. These spectra are very similar to the PL spectra in Fig. 5(a) and the peaks of the same wavelengths were numbered with the same letters (a–g). The main changes between PL and CL spectra are the following: Peak a from the thick QWR appears at a shifted energy, and accordingly, is marked a2. Peak e, related to intermediate {311} planes, does not appear in either spectrum 2 or 3; this is related to the higher spatial resolution of the CL system and the limited spatial extent of this peak. Due to the same reason, peaks c and h, which appear in spectrum 1 (and belong to the narrow V groove), are missing in spectra 2 and 3.

The CL systems lets us to acquire wavelength-dispersive CL *images* of the QWR samples, thus allowing more precise localization of the spatial extent and structural feature associated with each spectral feature. To this end, we took a series of CL images of an array of 1-μm-pitch QWRs, with 10-μm space between wide parts, as shown in Fig. 6(b). The detection wavelengths in each picture correspond to one of the PL/CL peaks in Figs. 5(a) and 6(a) and are marked with the corresponding letter (a–g).

The lowest-energy luminescence peak (a2), at 1.565 eV, originates from the center of the wide part of the groove. The *width* of the luminescence area (averaged from 20 regions) is 450 ± 50 nm. However, we know from the AFM cross-sectional study (Fig. 2) that the real *width* of the luminescing region at this wavelength range, i.e., a quantum wire, is only on the order of 10–20 nm, so its apparent width is a good measure of the excitation area of the electron beam (=effective CL resolution). The length of the area (averaged from 20 regions) is 0.95 ± 0.25 μm, which corresponds to the length of the entire wide part of the groove. This points to an effective carrier transfer to the QWR from the AlGaAs volume of the wide part, and possibly from the QWs in the wide part, but not beyond this range. This ''cut out'' could be associated with the transition from {311} *A* planes in the intermediate zone [Fig. 2(F)], where the effective gap in the QW is larger than in the QWRs [Fig. 2(F)]. A CL image taken at 1.55 eV, corresponding to PL peak a1, is almost identical to the one taken at 1.565 eV, but shows lower intensity; the luminescence at the two wavelengths could be due to peak width [e.g., in Fig. 6(a), the CL intensity at 1.55

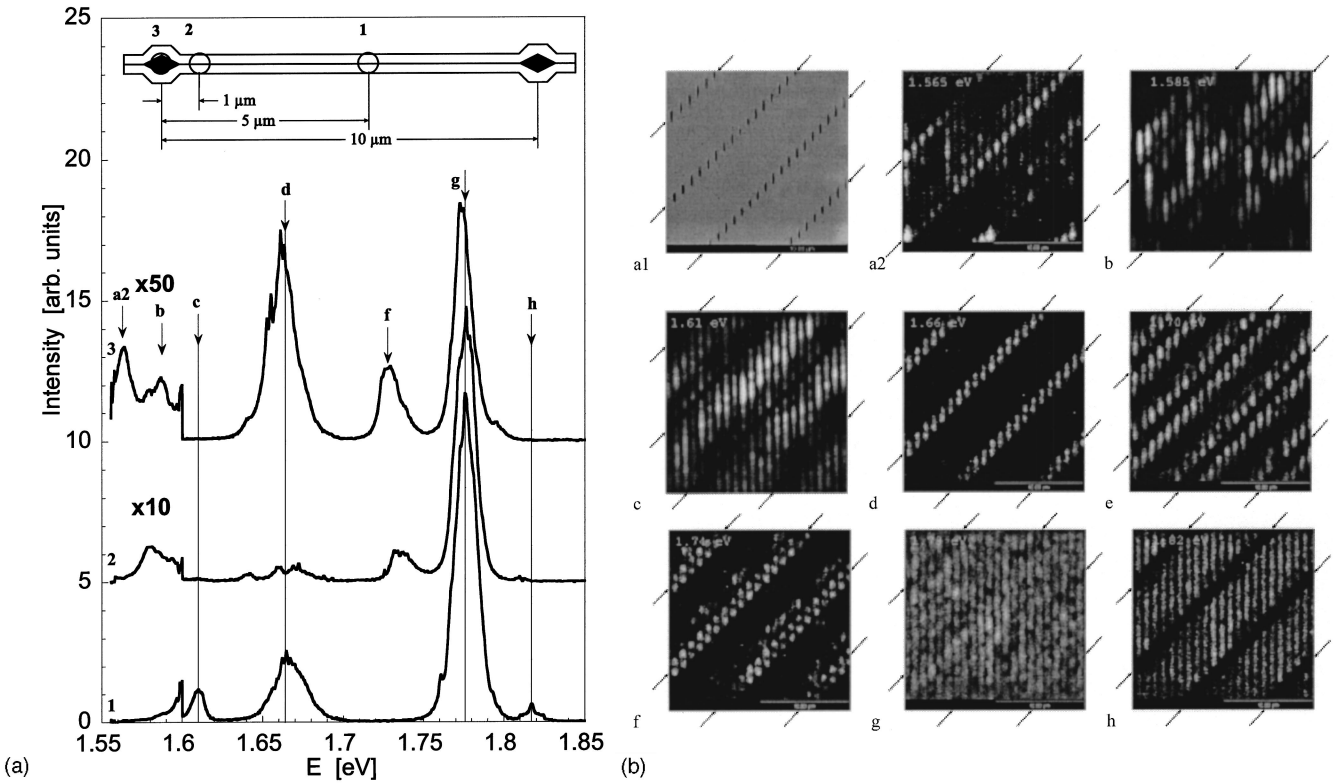

FIG. 6. (a) CL spectra at $T=10$ K, taken at three different positions along a variable-width structure (spectra 1–3), as indicated in the inset diagram (the circles show the approximate size of the CL excitation area, 0.4 μm; the wide QWR size is exaggerated). The arrows marking a–g denote peaks and groups of peaks that are referred to in the text. (b) SEM secondary electron image (top left) and a series of CL images of a variable-width QWR array. The grooves are vertical, with a horizontal pitch of 1 μm, and the wide parts are spaced at 10-μm intervals (along the grooves) and displaced by 1 μm along the groove to form a diagonal pattern. All CL images are taken at the same magnification ($\times$3400), but at different detection wavelengths: (a1) SE image; (a2) CL, 1.565 eV; (b) CL, 1.585 eV; (c) CL, 1.61 eV; (d) CL, 1.66 eV; (e) CL, 1.70 eV; (f) CL, 1.74 eV; (g) CL, 1.78 eV; (h) CL, 1.82 eV. To help localize the structural features in the images, the diagonal rows of wide grooves are denoted by arrows.

eV is not zero] or perhaps due to luminescence from higher QWR subbands.

As we already mentioned, peak b at 1.585 eV in the PL spectrum can be attributed to the QWR just outside the wide part and extending about 2.0 ± 0.4 μm beyond it. From the image it can be seen that this luminescence segment is clearly separated from the QWR in the wide part. When the detection wavelength is increased to 1.61 eV (peak c), the QWR in the central part of the narrow groove luminesces. This central segment has a length on the order of 5 μm, and is similar in luminescence energy to ''standard'' QWRs grown in narrow V grooves. The difference between peaks b and c leads us to believe that there is some thickening of the QWR towards the wide part, lowering the CL energy, due to longitudinal Ga diffusion during growth.

Higher-energy features (peaks d–g) are related to quantum wells at different parts of the structure. For example, the relatively localized spectral features at 1.66 (d) and 1.74 eV (f), which are composed each of two segments in the wide region (but not exactly at its center), are probably related to the {311} *A* and {111} *A* side QWs, respectively, both in the intermediate part of the wide region. As we saw in the PL/CL spectra, peak d exists also in the spectrum from the narrow part [e.g., spectrum 1 in Fig. 6(a) taken from the *same* sample]; however, its height is lower there, making it less visible in the CL image of the narrow part.

At an emission energy of 1.70 eV (e) we observe the {311} *A* facet luminescence of the outer part of the narrow V groove. The energy difference between peaks d and e could also be attributed to the same Ga diffusion described above being responsible for the differences between peaks a and b. The {100} ridge (top) QWs between the grooves can be identified on the CL images taken at 1.78 eV (g). This spectral feature is very uniform in the image, and is present everywhere except (of course) at the center of the groove, where the QWR passes.

Finally, at 1.82 eV (h), only the center of the narrow part emits. This feature can be attributed to the vertical QW (VQW) since the emission energy corresponds to the emission of an AlGaAs alloy containing about 20% Al. This is a typical Al concentration in a VQW that is formed in a $Al_{0.3}Ga_{0.7}As$ at these growth conditions.[32] More accurate modeling shows the Al concentration to be 31.5% in the cladding and 20% in the VQW. In the wide part there is no VQW emission since the structure is less planarized there, hence the VQW is very short and carrier transfer is therefore very fast to the QWR.

TABLE I. Correlation between peak energies in PL and CL spectra (Figs. 5 and 6) and structural features observed by AFM (Fig. 2). For each peak, the effective QWR or QW thicknesses were calculated and compared with measured AFM thicknesses (scaled to the nominal GaAs layer thickness). The error bars correspond to the accuracy of our model calculation (for QWs) or interpolation (for QWRs).

Peak number	Placement	Type	Peak energy (eV)	PL thickness (nm)	AFM thickness (nm $\pm$ 0.5)	Identification
a1	center of wide	QWR	1.55 (PL),	11.6 $\pm$ 1,	11.2	thick QWR at center
a2	part		1.565 (CL)	9.4 $\pm$ 1		of wide part
b	narrow groove, outside center	QWR	1.585	6.7 $\pm$ 0.7		thickened QWR in narrow part
c	narrow groove, center	QWR	1.61	4.3 $\pm$ 0.5	4.4	''standard'' QWR in narrow part
d	narrow groove	QW	1.66	4.1 $\pm$ 0.2	3.8	side QW {311}
e	outside wide part	QW	1.695	3.4 $\pm$ 0.2	3.6	side QW {311}
f	outside wide part	QW	1.74	2.7 $\pm$ 0.2	2.2	side QW {111}
g	narrow groove	QW	1.77	2.2 $\pm$ 0.2	2.0	top QW
h	narrow groove	QW	1.82	7 $\pm$ 0.2		vertical WQ

VI. LINKING STRUCTURAL AND SPECTRAL FEATURES

The complexity of the structure, as observed by the AFM cross-sectional study (Fig. 2), leads naturally to the very rich PL/CL spectra described above (Figs. 5 and 6). Most of the spectral features were linked to specific parts of the structure by observation of the spectrally resolved CL images. To further test these assignments, we tried to deduce from the AFM study the thickness of QW or QWR related to each spectral feature, and compare it to the thickness inferred from the peak energy observed in PL and CL spectra. In doing so, we scaled the width of each structural feature, as measured in the AFM images (Fig. 2), according to the ratio of nominal GaAs grown thickness (5 nm in the AFM sample; 1.5 nm in the PL sample). The QW widths were deduced from a simple finite quantum well model, using the Al mole fraction (31.5%) measured by x-ray diffraction and corresponding to the VQW luminescence. In the QW model we took into account the different electron and hole effective masses in GaAs and AlGaAs, but neglected crystal anisotropy and excitonic effects. The QWR widths were deduced by interpolation between the data of several uniform QWRs of the same Al mole fraction as our samples and of different sizes, which have been measured in the past in our laboratory,[31] therefore, the results show larger error bars. The results are summarized in Table I and in Fig. 7 where we plot the QW and QWR thicknesses (from both AFM and PL data) as a function of PL peak energy. The peaks are marked by the same letters used in Figs. 5 and 6. The overall correspondence between AFM and PL data is quite good, especially for the QWs, thus supporting the validity of our peak identification. The thick QWR AFM data show better correspondence with peak a1 (1.55 eV) of the PL spectrum; as we suggested previously, peak a2 could be a higher subband, excited by the high CL current. As for peak b, since we assume that it results from thickening of the ''uniform'' QWR in the narrow groove, it is situated outside the range of the AFM cross-sectional range, so no data was available for comparison.

VII. CONCLUSIONS

We have developed a method for fabrication of mixed dimensionality heterostructures by OMCVD growth in axially modulated V grooves fabricated by EBL. Our method combines the flexibility and precision of EBL with the clean, defect-free interfaces of small-size QWRs grown by

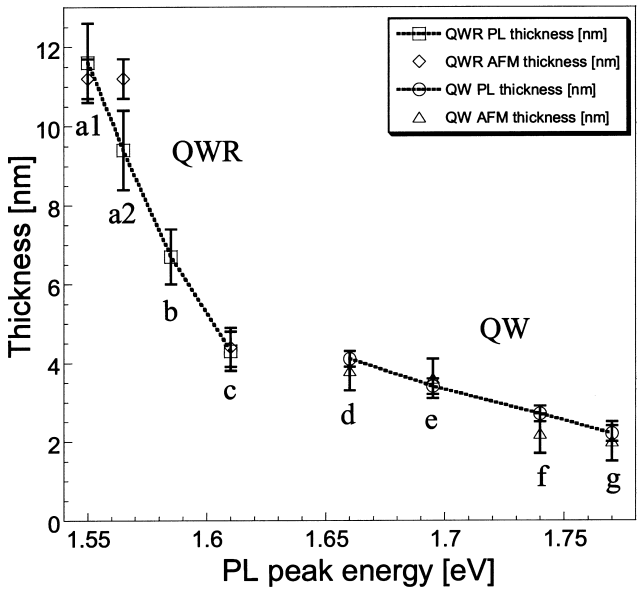

FIG. 7. QW and QWR thicknesses, as calculated from the position of PL-peaks in Fig. 5(a) (marked a–h), compared to measured thicknesses from the AFM images in Fig. 2 (scaled to the grown GaAs layer thicknesses). The error bars correspond to AFM measurement accuracy (QW and QWR AFM), model accuracy (QW PL), and interpolation accuracy (QWR PL). The dotted lines are guides to the eye.

OMCVD in grooved substrates. We showed that growth of AlGaAs/GaAs heterostructures in grooves of varying widths leads to the formation of narrow and wide crescent-shaped QWRs at the bottom of the narrow and wide parts of the groove, respectively. These QWRs are accompanied by QWs, growing along the {311} *A* and {111} *A* facets. Mass transport along the groove leads to the thickening of the GaAs QWR in the center, as well as to significant shrinking in its length and in the size of the wide parts of the groove. These growth modes can be used to produce different types of nanostructures, such as short and thick QD-like sections, as well as different QWs and QWRs.

Measurements of photo- and cathodoluminescence spectra showed the signature of all structural features, and corroborated their identification by AFM. Specifically, they confirmed the formation of a short, QD-like segment of a thicker QWR at the center of the wide part of the groove, with band-gap energy lower by up to 50 meV than that of the self-limited QWR. However, the strong faceting of the substrate and grown structure could prevent the efficient transfer of carriers along the QWR to the wider part, at least at low temperatures and for the thin GaAs layer thickness used.

These structures could be eventually used in several ways in either fundamental or applied studies, e.g., by using the QW with thickened edges (Fig. 2) as a double QWR in a Bohm-Aharonov interferometer scheme, or by combining {311} and {111} QWs with amphoteric dopants to create electron and hole gases at close distances. These structures could open the way to experiments in mixed dimensionality (QW-QWR-QD) structures.

ACKNOWLEDGMENTS

We wish to thank E. Martinet, D. Oberli, F. Vouilloz, and T. Otterburg for their help in PL measurements, as well as F. Reinhardt for growing the samples. This work was supported in part by the Fonds National Suisse de la Recherche Scientifique.

[1] Y. Arakawa and H. Sakaki, Appl. Phys. Lett. **40**, 939 (1982).
[2] C. Weisbuch and B. Winter, *Quantum Semiconductor Structures* (Academic, Boston, 1991).
[3] R. Nötzel, N. N. Ledentsov, L. Däweritz, M. Hohenstein, and K. Ploog, Phys. Rev. Lett. **67**, 3812 (1991).
[4] M. Kasu and N. Kobayashi, Appl. Phys. Lett. **62**, 1262 (1993).
[5] G. A. Lyubas, N. N. Ledentsov, D. Litvinov, D. Gerthsen, I. P. Soshnikov, and V. M. Ustinov, Pis'ma Zh. Eksp. Teor. Fiz. **75**, 211 (2002) [JETP Lett. **75**, 179 (2002)].
[6] A. Yacoby, H. L. Stormer, K. W. Baldwin, L. N. Pfeiffer, and K. W. West, Solid State Commun. **101**, 77 (1997).
[7] A. Gustafsson, F. Reinhardt, G. Biasiol, and E. Kapon, Appl. Phys. Lett. **67**, 3673 (1995).
[8] A. Crottini, J.-L. Staehli, B. Deveaud, X.-L. Wang, and M. Ogura, Phys. Rev. B **63**, 121313(R) (2001).
[9] G. Biasiol and E. Kapon, Phys. Rev. Lett. **81**, 2962 (1998); F. Lelarge, G. Biasiol, A. Rudra, A. Condo, and E. Kapon, Microelectron. J. **30**, 461 (1999).
[10] F. Lelarge, T. Otterburg, D. Y. Oberli, A. Rudra, and E. Kapon, J. Cryst. Growth **221**, 551 (2000).
[11] D. Kaufman, Y. Berk, B. Dwir, A. Rudra, A. Palevski, and E. Kapon, Phys. Rev. B **59**, R10 433 (1999).
[12] F. Vouilloz, S. Wiesendanger, D. Y. Oberli, B. Dwir, F. Reinhardt, and E. Kapon, Physica E (Amsterdam) **2**, 862 (1998).
[13] P. Exner, Phys. Lett. A **141**, 213 (1989); P. Exner and P. Seba, J. Math. Phys. **30**, 2574 (1989).
[14] J. Goldstone and R. L. Jaffe, Phys. Rev. B **45**, 14 100 (1992).
[15] J. P. Carini, J. T. Londergan, K. Mullen, and D. P. Murdock, Phys. Rev. B **48**, 4503 (1993).
[16] C. S. Lent and D. J. Kirkner, J. Appl. Phys. **67**, 6353 (1990).
[17] J. P. Carini, J. T. Londergan, K. Mullen, and D. P. Murdock, Phys. Rev. B **46**, 15 538 (1992).
[18] J. P. Carini, J. T. Londergan, D. P. Murdock, D. Trinkle, and C. S. Yung, Phys. Rev. B **55**, 9842 (1997); **55**, 9852 (1997).
[19] A. Weisshaar, J. Lary, S. M. Goodnick, and V. K. Tripathi, Appl. Phys. Lett. **55**, 2114 (1989).
[20] H. U. Baranger, Phys. Rev. B **42**, 11 479 (1990).
[21] S. Mendoza, M. del Castillo-Mussot, and W. L. Mochan, Phys. Rev. B **53**, 1026 (1996).
[22] A. A. Odintsov, Y. Tokura, and S. Tarucha, Phys. Rev. B **56**, R12 729 (1997).
[23] D. Kaufman, B. Dwir, A. Rudra, A. Palevski, and E. Kapon, Physica E (Amsterdam) **7**, 576 (2000).
[24] J. C. Wu, M. N. Wybourne, W. Yindeepol, A. Weisshaar, and S. M. Goodnick, Appl. Phys. Lett. **59**, 102 (1991).
[25] R. Bergmann, H. Schweizer, V. Härle, and F. Scholz, Appl. Phys. Lett. **68**, 2267 (1996).
[26] F. Perez, B. Jusserand, C. Dahl, M. Filoche, L. Ferlazzo-Manin, and B. Etienne, Phys. Rev. B **54**, R11 098 (1996).
[27] F. Reinhardt, B. Dwir, and E. Kapon, Appl. Phys. Lett. **68**, 3168 (1996).
[28] B. Dwir, F. Reinhardt, A. Gustafsson, H. Weman, and E. Kapon, Microelectron. Eng. **35**, 269 (1997).
[29] V. Türk, O. Stier, F. Heinrichsdorff, M. Grundmann, and D. Bimberg, Phys. Rev. B **55**, 7733 (1997).
[30] F. Lelarge, D. Kaufman, B. Dwir, S. Mautino, A. Rudra, and E. Kapon, J. Cryst. Growth **221**, 540 (2000).
[31] F. Vouilloz, Ph.D. thesis, Swiss Federal Institute of Technology, 1998.
[32] G. Biasiol, Ph.D. thesis, Swiss Federal Institute of Technology, 1998.